Dependence of Fluorescence Intensity on the Spectral Overlap between Fluorophores and Plasmon Resonant Single Silver Nanoparticles

Yeechi Chen, Keiko Munechika, and David S. Ginger*

Department of Chemistry, University of Washington, Seattle, Washington 98195-1700

ABSTRACT

We investigate the fluorescence from dyes coupled to individual DNA-functionalized metal nanoparticles. We use single-particle darkfield scattering and fluorescence microscopy to correlate the fluorescence intensity of the dyes with the localized surface plasmon resonance (LSPR) spectra of the individual metal nanoparticles to which they are attached. For each of three different dyes, we observe a strong correlation between the fluorescence intensity of the dye and the degree of spectral overlap with the plasmon resonance of the nanoparticle. On average, we observe the brightest fluorescence from dyes attached to metal nanoparticles that have a LSPR scattering peak ∼40−120 meV higher in energy than the emission peak of the fluorophore. These results should prove useful for understanding and optimizing metal-enhanced fluorescence.
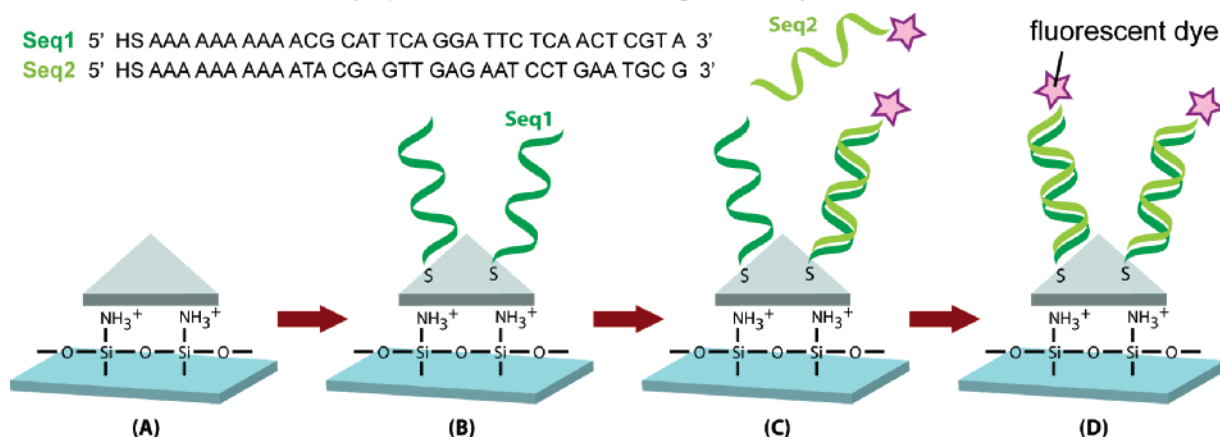
Metal nanoparticles and nanostructured metal films possess localized surface plasmon resonances (LSPRs) that imbue these materials with a number of unique and useful optical properties. LSPRs are responsible for the size- and shape-dependent optical spectra that have led to the use of metal nanoparticles in a variety of biodiagnostic applications,[1,2] and plasmon modes have been implicated in the extraordinary transmission of light through nanoscale hole arrays.[3] Furthermore, the highly confined local electric field enhancements that accompany the excitation of LSPRs are used in a variety of near-field enhanced spectroscopy and imaging modes, from near-field scanning optical microscopy[4−6] to surface-enhanced Raman spectroscopy (SERS).[7−10]

Although SERS applications have motivated much of the research into surface-enhanced spectroscopy in the past decade, the widespread use of fluorescence-based sensing in biology and the importance of radiative decay near metal electrodes in organic optoelectronics[11,12] are two factors that have led to a great deal of new interest in the study of simple fluorescence near metal nanostructures.[2] Although planar metal films generally quench the emission from nearby fluorophores,[13,14] the effects of metal nanostructures are more complicated. Depending on the details of the system under investigation, fluorescence quenching,[15−17] enhancement,[18−23] or both,[24] have been reported in experimental studies of fluorescent dyes and quantum dots near nanostructured metals. While the increased surface area (and hence the increased amount of adsorbed dye) of a nanostructured metal surface compared with a planar substrate might account for some of the reports of enhancement, the observation of enhancement in single-molecule experiments[17,22−24] and planar dye layers with adsorbed nanoparticles[18] indicates that real, nontrivial enhancements of fluorescence using near-field effects are achievable. The origins of such nontrivial fluorescence enhancement effects near nanostructured metal can be understood as arising from two contributions. First, by concentrating the incident light into local electromagnetic "hot spots", nanostructured surfaces can lead to increased absorption of the incident light by the fluorophores. Second, metal nanostructures can alter the radiative and the nonradiative decay rates of nearby fluorophores, changing both the fluorescence lifetime and quantum yield. Although it has remained difficult to separate the effects of excitation and emission enhancement, both of these local field effects are expected to be extremely sensitive functions of the shape of the metal particle, the orientation of the dye, and the distance between the dye and the metal,[25−29] just as they are for dyes attached to planar metal films.[13,14] Many groups have studied variation in fluorescence intensity as a function of the distance between a layer of fluorophores and a number of nanostructured metal surfaces,[30,31] adsorbed colloidal particles,[20] or suspended colloidal particles.[15,32,33] Single-molecule experiments have even provided strong evidence for the existence of a local maximum in the fluorescence intensity versus distance curve.[23,24]

* Corresponding author. E-mail: ginger@chem.washington.edu. Telephone: (206)685-2331. Fax: (206)685-8665.

Scheme 1. Creating Dye-functionalized Silver Nanoprisms Using DNA as a Structural Linker

Seq1 5′ HS AAA AAA AAA ACG CAT TCA GGA TTC TCA ACT CGT A 3′
Seq2 5′ HS AAA AAA AAA ATA CGA GTT GAG AAT CCT GAA TGC G 3′

(A) Silver nanoprisms are immobilized on a silanized glass slide. (B) A ssDNA monolayer is attached to the nanoprisms via a 5′ thiol group. (C) Complementary DNA conjugated with a fluorescent dye is hybridized to the DNA-functionalized nanoprisms, resulting in (D) specific attachment of the dye at a finite distance from the nanoprism surface.

In addition to this distance dependence, local field enhancements surrounding metal nanostructures are strongly wavelength dependent,[34] and one expects that the amount of fluorescence enhancement or quenching will also depend on the spectral overlap between the dye and the LSPR modes of the nanoparticle. However, the effects of spectral overlap have been less studied.[23,35] This lack of investigation is partly due to the broad extinction peaks exhibited by many inhomogeneous and partially aggregated metal films. Even studies on colloidal solutions must contend with inhomogeneously broadened spectra. Several groups have recently used ion- or electron-beam lithography to produce arrays of holes or nanoparticles to study metal-enhanced fluorescence. While these studies have demonstrated some correlation between fluorescence intensity and the size, shape, and spacing of the metal nanostructures[36−39] as well as with the spectral properties of nanohole[37] and nanoparticle[39] arrays, the spectral linewidths of these arrays are still quite broad (∼100+ nm fwhm) and incorporate both near-field and diffractive coupling effects due to the regular lattice, making it difficult to differentiate between enhancement of fluorophore excitation or emission and changes in the angular emission profile due to a periodic particle array. Furthermore, many of these studies disperse the fluorophores in polymer films[37−39] up to 30 nm thick, averaging over both the distance and spectral overlap effects. Kühn et al. have studied enhancement from well-controlled single molecule−nanoparticle systems but were spectrally limited to a single plasmon resonance peak and a single fluorophore.[23]

To obtain a better understanding of the impact of metal nanostructures on nearby fluorophores, it is desirable to study many systems with both well-defined metal−fluorophore distances and narrow spectral features. In this work, we describe such an experimental approach based on the fluorescence of dyes attached at a fixed distance from single silver nanoparticles using DNA as a biological linker[15,40,41] (Scheme 1). We then employ single-particle darkfield scattering spectroscopy and fluorescence microscopy to better

study the impact of spectral overlap between the metal nanostructures and the attached dyes. After removing inhomogeneous broadening, scattering resonances of individual colloidal metal nanoparticles can be much narrower than the ensemble solution spectra[42,43] and are limited primarily by lifetime broadening.[44] Thus, we are able to correlate the fluorescence intensity of the adsorbed dyes with the spectral properties of the underlying metal nanoparticles with significantly greater precision than in previous reports. We provide measurements that should be useful for comparison with recent calculations, as well as for the selection of colloid syntheses and lithographic structures best paired with dyes in fluorescence applications.

For the purpose of this work, we chose to couple fluorophores to highly anisotropic silver nanoprisms with large scattering cross-sections and plasmon resonances that are tunable across the visible spectrum.[42,43] Such particles exhibit larger local field enhancements than spherical particles[34] and their sharp edges lead to more effective coupling of the LSPR to far-field radiation.[43] They are thus more promising candidates for fluorescence studies than spherical particles. We synthesized silver nanoprisms following literature procedures;[45] full details are available as Supporting Information. Although a variety of sizes and shapes are produced, the synthesis yields mostly triangular silver nanoprisms with edge lengths of 100 ± 20 nm (Figure 1) and thicknesses of approximately 12 nm (Supporting Information, Figure S3), consistent with previous reports.[45] Following Scheme 1, we isolated individual nanoparticles for single-particle spectroscopy by attaching them to no. 1 thickness glass coverslips treated with 3-aminopropyltrimethoxysilane (APTMS). A dilute solution (optical density ∼0.2 at 640 nm) of nanoprisms was then placed on the silanized coverslip for a period of minutes, after which unbound nanoprisms were rinsed off with water and the substrate was dried with a stream of nitrogen. The attachment time, typically 3 min, was adjusted to yield final densities of ∼20 or fewer nanoprisms per 100 μm^2, well-isolated to facilitate single-particle spectroscopy.
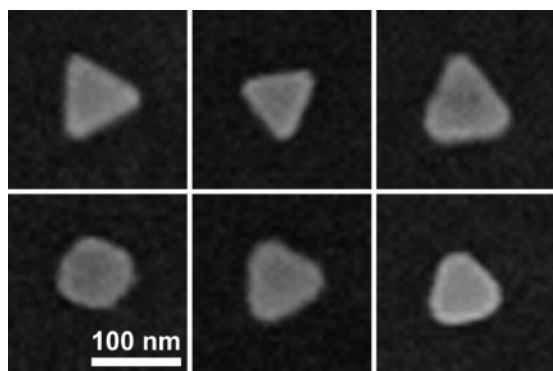
Figure 1. Collage of SEM images showing the typical range of sizes and shapes for the silver nanoprisms used in these experiments. There is some size and shape variation, and the corners exhibit varying degrees of truncation.

We then used double-stranded DNA (dsDNA) to couple fluorescent dyes to the nanoprisms (Scheme 1). DNA is a promising spacer molecule[46] well-suited to distances relevant to near-field fluorescence.[15] Although a single fixed length was used for this study, DNA-linked dyes also offer the possibility of varying the fluorophore metal spacing by changing the length of the DNA. For this work, we used two complementary strands of 34-mer DNA sequences, synthesized and HPLC purified by Integrated DNA Technologies (Coralville, IA). Each sequence was functionalized at the 5′ end with a thiol group. *Seq1* (5′ HS AAA AAA AAA ACG CAT TCA GGA TTC TCA ACT CGT A 3′) was used to form a self-assembled monolayer of single-stranded DNA (ssDNA) on the nanoprism surface (Scheme 1B) following procedures developed for planar surfaces.[47] The complementary sequence *Seq2* (5′ HS AAA AAA AAA ATA CGA GTT GAG AAT CCT GAA TGC G 3′) was conjugated with one of three thiol-reactive dyes (Alexa Fluor 488 C_5-maleimide, Alexa Fluor 532 C_5-maleimide, Rhodamine Red C_2-maleimide) obtained from Molecular Probes (Invitrogen, Portland, OR) and purified prior to hybridization to the DNA-functionalized nanoprisms. Detailed descriptions of the attachment and hybridization protocols are available in the Supporting Information.

Figure 2A shows a dark-field optical microscopy image of a typical field of silver nanoprisms. The variation in scattered nanoparticle colors arises from the inhomogeneous size and shape distributions of the colloidal particles. We obtained LSPR scattering spectra from individual silver nanoparticles using a fiber-coupled CCD spectrometer as described in the Supporting Information. The normalized scattering spectra from several particles identified in Figure 2A are shown in Figure 2B. The individual LSPR line widths range from 30 to 80 nm, consistent with previous reports,[42,43,48] and are considerably narrower than the solution ensemble extinction spectrum (dashed and shaded trace in Figure 2B). The LSPR peak positions fall within the envelope of the ensemble spectrum.

Significantly, we achieve good specific attachment of the fluorophores to the silver nanoprisms via DNA hybridization. Figure 3A shows a darkfield micrograph of a field of silver nanoparticles just prior to being functionalized with ssDNA
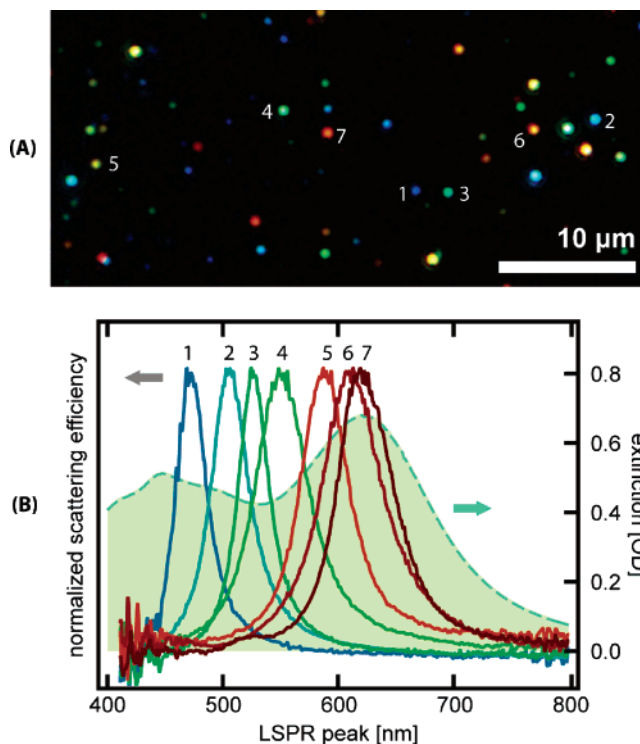

Figure 2. (A) Darkfield optical micrograph of a typical distribution of silver nanoparticles immobilized on a glass coverslip. (B) Single-particle darkfield scattering spectra corresponding to the individual silver nanoprisms labeled in (A). The ensemble solution extinction spectrum is shown as the shaded, dashed curve for comparison.

(*Seq1*). Figure 3B shows a fluorescence micrograph of the same region after attachment of the thiolated-DNA monolayer and incubation of the substrate with noncomplementary Rhodamine Red-conjugated DNA (*Seq1*). Only very low fluorescence (due to minor amounts of nonspecific binding) is detectable either on the background or the DNA-coated nanoparticles. In contrast, Figure 3C shows an identical exposure of the same region of the substrate after it has been incubated with complementary dye-conjugated DNA (*Seq2* + Rhodamine Red). The background fluorescence remains low, and significant fluorescence is observed from the dye-functionalized nanoparticles, confirming the specific DNA-mediated attachment of the dyes. Using atomic force microscopy (AFM), we measured the thickness of the double-stranded DNA layer to be approximately 5.5 nm on the surfaces of the nanoprisms (Supporting Information, Figure S3), consistent with the thickness of comparable DNA layers on planar surfaces.[49] Although the hybridization is specific, there is a clear variation in the fluorescence intensity of the individual particles. We believe a major component of this variation is due to the different sizes and shapes of the silver nanoparticles (Figure 1). These size and shape variations produce shifts in individual LSPR resonances, which lead to different wavelength-dependent local field enhancement factors at the absorption and emission frequencies of the dye.

Using the DNA-based attachment chemistry, we are able to study the effects of spectral overlap in more detail. Figure 4A shows a darkfield image of a field of DNA-functionalized silver nanoparticles that have been incubated with a mixture of complementary dye-labeled DNA strands in order
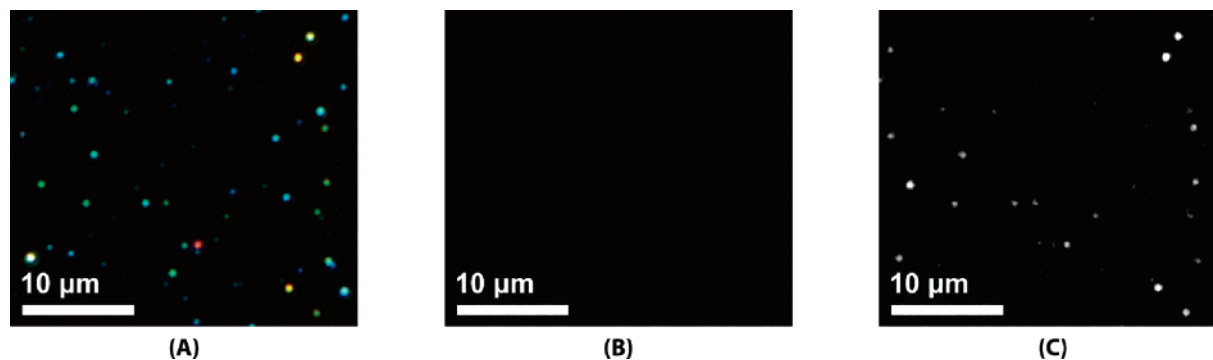
Figure 3. Specific DNA-directed coupling of fluorescent dyes with silver nanoprisms. (A) Darkfield optical micrograph showing a field of isolated silver nanoprisms. (B) Incubation of the DNA-functionalized particle field in (A) with noncomplementary dye-labeled DNA results in little detectable fluorescence. (C) Subsequent hybridization of the same sample with complementary Rhodamine Red-labeled DNA leads to attachment of the dye and visible fluorescence from the functionalized nanoparticles.
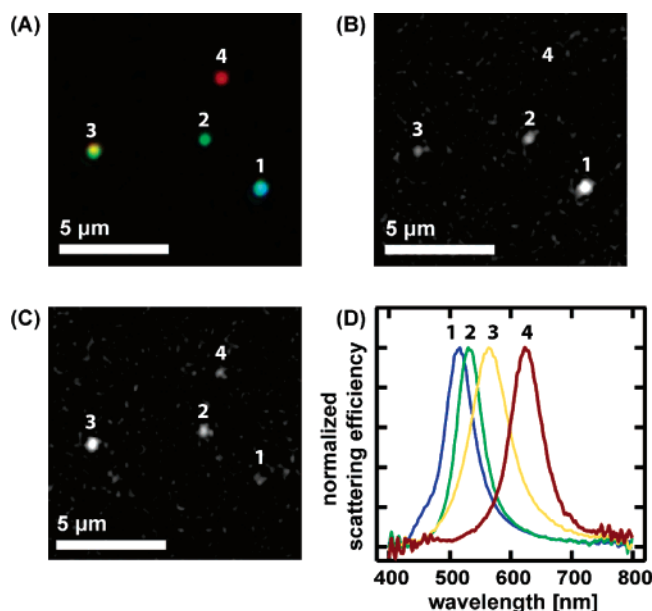

Figure 4. (A) Darkfield optical micrograph of four individual silver nanoparticles that have been hybridized with a 1:1 mixture of the dyes Alexa Fluor 488 and Rhodamine Red. (B) Fluorescence micrograph of the same area collected using Alexa Fluor 488 excitation and emission. (C) Fluorescence micrograph of the same area collected using Rhodamine Red excitation and emission. (D) Single-particle scattering spectra show the LSPR for each particle in (A).

to tag each particle with a one-to-one ratio of two different fluorescent dyes (Alexa Fluor 488 and Rhodamine Red). Figure 4B shows the fluorescence from Alexa Fluor 488, and Figure 4C shows the fluorescence from Rhodamine Red, both of which were isolated using appropriate filter sets (details of excitation, dichroic, and emission filter sets and lamp spectra are provided in Supporting Information). Noticeably, the yellow particle (no. 3) in the darkfield image (LSPR peak at 564 nm, Figure 4D) shows the most Rhodamine Red fluorescence (red-orange dye), but very little fluorescence from Alexa Fluor 488 (green dye). In contrast, the aqua-blue particle (no. 1) in the darkfield image (LSPR peak at 517 nm, Figure 4D) is by far the brightest particle in the image of the Alexa Fluor 488 dye fluorescence, while the yellow particle (no. 3), brightest in the Rhodamine Red

image, has barely visible fluorescence. These data provide clear experimental evidence that overlap of the nanoparticle LSPR with the spectra of the dye plays a key role in determining the brightness of the dye fluorescence at the level of an individual nanoparticle.

Using single-particle spectroscopy, we were also able to investigate the effects of spectral overlap in more quantitative fashion. To do so, we prepared many DNA-functionalized silver nanoparticle substrates and used DNA hybridization to attach one of the three fluorescent dyes (Alexa Fluor 488, Alexa Fluor 532, and Rhodamine Red) to the nanoparticles. Single-particle darkfield spectra were then obtained and correlated with the fluorescence intensity of the dye coupled to that particle. We obtained correlated spectra and fluorescence intensity measurements for 457 total single particles (N = 188, Alexa Fluor 488; N = 147, Alexa Fluor 532; N = 122, Rhodamine Red). These numbers include only spectra of particles with dominant single, narrow (fwhm < 80 nm) scattering peaks.

Parts A−C of Figure 5 show the resulting correlations by plotting the average fluorescence intensity as a function of the individual particle LSPR peaks, grouped in 20 nm bins. The excitation and emission spectra of the dyes are overlaid as the shaded curves in each plot for comparison. The dye emission spectra (shown for comparison) are taken from dye-conjugated DNA monolayers, intentionally adsorbed on glass coverslips in the absence of silver prisms, and are corrected for instrument response. The excitation spectra (shown for comparison) are taken from the dye-conjugated DNA in water (due to the difficulty of obtaining absorption data on dye monolayers).

Parts A−C of Figure 5 summarize the key experimental findings of this work and show that the fluorescence intensity of a dye absorbed to a silver nanoparticle is strongly dependent on the overlap between the LSPR of the nanoparticle with the spectral properties of the dye. The maximum fluorescence from Alexa Fluor 488 is observed when coupled to particles with LSPR peaks at ∼505 nm. For Alexa Fluor 532, the maximum fluorescence is observed when coupled to particles with LSPRs at ∼525 nm, while for Rhodamine Red, the brightest fluorescence is observed when the dye is absorbed to particles with LSPR peaks at ∼570 nm. For each
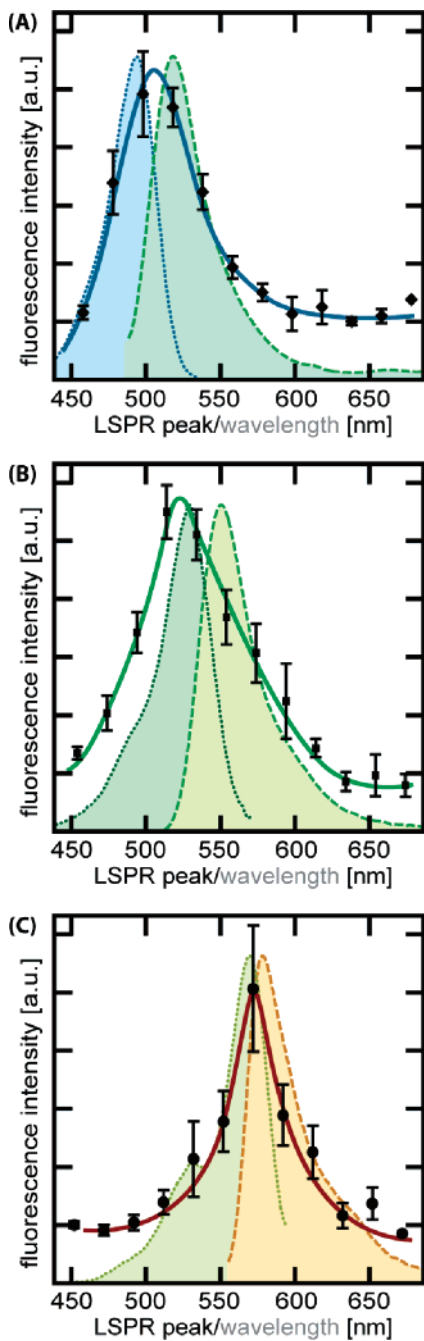
Figure 5. Summary of 457 individual particle fluorescence vs LSPR peak position measurements with three different fluorescent dyes. The LSPR peak positions are binned in 20 nm intervals along the x-axis. The average fluorescence intensity observed from particles within each bin is then plotted as a function of the LSPR position for silver nanoprisms functionalized with (A) Alexa Fluor 488, (B) Alexa Fluor 532, and (C) Rhodamine Red dyes. The excitation spectra (dotted lines) and emission spectra (dashed lines) are plotted for reference for each dye. The solid line is a guide to the eye. Y-error bars represent the standard deviation of the mean fluorescence intensity observed from particles with LSPR peaks within each 20 nm bin.

dye, the relative *average* brightness ratio "on" and "off" the maximum fluorescence peak is about 5−7. We estimate the absolute fluorescence enhancement factor (versus an equal number of free dye molecules) to be 9−30 for the brightest *individual* particles (obtained by determining the ratio of the

fluorescence intensities of the dye-labeled nanoparticle with the intensity of a single dye molecule and correcting for the number of dyes on each nanoparticle; see Supporting Information).

We can understand the strong spectral correlation shown in Figure 5 if we write the apparent brightness of a fluorophore functionalized metal nanoparticle, Y_{APP}, as:

$$Y_{APP} = \gamma_{ex}(\omega_{ex})Q_{EM}(\omega_{em})\eta_{coll}(\omega_{em})\sigma \quad (1)$$

where $\gamma_{ex}(\omega_{ex})$ is the near-field excitation rate of the fluorophores at the excitation frequency ω_{ex}, $Q_{EM}(\omega_{em})$ is the quantum yield for far-field emission at the emission frequency ω_{em}, $\eta_{coll}(\omega_{em})$ is the collection efficiency of the far-field light in the experimental geometry (accounting for any modification of the free-space spatial emission profile and the fixed angular acceptance of the detector) and σ is a normalization factor accounting for attachment density and total area excited. Although straightforward, the σ and $\eta_{coll}(\omega_{em})$ factors in eq 1 are often neglected, and we include them for completeness; in our experiments with approximately similar particles sizes and shapes, we expect these variations to be of secondary importance. The near-field excitation rate, $\gamma_{ex}(\omega_{ex})$, will depend on both the absorption coefficient of the dye and the local (nanoparticle-enhanced) field intensity. Because the near-field enhancement is strongly frequency dependent, the highest excitation rate should occur for dyes adsorbed on nanoparticles with an LSPR peak that directly overlaps the maximum in the absorption spectrum of the dye. On the other hand, $Q_{EM}(\omega_{em})$ is also strongly frequency dependent: not only can the metal-altered local photonic mode density lead to changes in the radiative decay rate of the fluorophore, but the presence of the metal also opens up new nonradiative decay pathways via energy transfer to metal surface plasmon modes.[14, 26−28,50] However, the energy transferred to the metal as plasmon modes can also be rescattered into the far-field by either the coupling provided by the nanoparticle size and shape or through grating coupling in periodic planar structures.[14] Thus, a metal nanostructure can lead to either an increase or a decrease in the fluorescence quantum efficiency of a nearby fluorophore.

Although these varying effects have been invoked to explain previous studies of fluorescence near nanostructured metals,[15−17,22−24] our correlation of many single-particle LSPR spectra and the fluorescence intensity of different absorbed dyes provides a new demonstration of the importance of spectral overlap between the LSPR and nearby fluorophores. Significantly, the data allow us to experimentally determine the optimum LSPR position for maximum fluorescence when using organic fluorophores with high free-space fluorescence quantum yields. For all three dyes, the brightest fluorescence is observed when they are attached to nanoparticles with LSPR peaks at higher energy than the dye emission peak. Specifically, the emission is brightest for dye−particle combinations for which the dye emission is red-shifted by ∼40−120 meV (Alexa Fluor 488, ∼70 meV; Alexa Fluor 532, ∼120 meV; Rhodamine Red, ∼40

meV) from the LSPR peak. This observed offset is in good qualitative agreement with recent calculations predicting the brightest fluorescence from dyes with emission peaks slightly red-shifted from the LSPR peak.[29] The optimum LSPR offset from the dye emission maximum appears to be slightly smaller than the Stokes shift for each dye: for two of the three dyes studied, the maximum brightness occurs when the LSPR peak is in between the dye absorption and emission maxima. Each dye is chemically distinct, and these variations in optimal spectral offset may depend on the different quantum yields, local environmental sensitivity, packing density, and position of the excitation and emission bands. Nevertheless, for all three dyes, the most fluorescence intensity is observed when the dye emission peak is red-shifted from the LSPR peak.

Although there is scatter in the data, and the Stokes shifts of the dyes are relatively small, the optimal LSPR location between the absorption and emission maxima could be explained if both the dye excitation and emission rates are being enhanced. Even though we expect excitation enhancement to dominate for fluorophores with high free-space quantum yields, this hypothesis is consistent with the results of Rothberg and co-workers,[18] which showed both excitation and emission effects contribute to the average fluorescence enhancement observed with random colloidal films. This hypothesis is also reminiscent of the SERS work by McFarland et al., which showed maximum SERS enhancement when both incident and Raman scattering photons experience local electromagnetic field enhancements.[51] We note the combination of excitation and emission enhancement for our high quantum-yield dyes could also explain the slight differences between our results, and the very recent work of Tam et al., who found that overlap between the LSPR and the emission spectra is the most important factor for low quantum yield dyes.[35] In future experiments, excitation and emission effects should be easier to differentiate using fluorophores with large Stokes shifts such as quantum dots.

Finally, we do see variations in the fluorescence intensity for dyes adsorbed to different particles with similar LSPR maxima. It is possible that these are due to variations in dye attachment density and/or orientation, but we believe that shape inhomogeneity also plays an important role, and we are currently studying the effects of nanoparticle shape on the fluorescence of the attached dyes in hopes of answering this question.

In conclusion, we have used DNA as a biological linker to attach fluorescent dyes at a fixed distance from single silver nanoprisms. The dye-functionalized nanoprisms are highly fluorescent, and their fluorescence intensity is a sensitive function of the degree of spectral overlap between the nanoparticle LSPR and the absorption and emission spectra of the dye. The DNA/silver nanoprism system is particularly promising for the study of near-field enhancement effects, and we anticipate that future work will examine the fluorescence emission and lifetime as a function of both dye-to-prism distance and spectral overlap. In this work, we have shown that, for dyes attached to ~5.5 nm thick DNA layers, the brightest fluorescence is usually obtained near nanoparticles with LSPR peaks that are only slightly blue-shifted from the dye emission peak. Not only do these results appear to validate recent theoretical predictions,[29] but they provide concrete empirical guidelines for selecting the best metal colloids as supports for particular fluorescence applications. We expect these results will benefit attempts to use metal-enhanced fluorescence in both biosensing[1,2] and thin-film optoelectronics applications.[11,12]

Supporting Information Available: Detailed experimental procedures; intermediate stages of sample characterization; experimental apparatus; spectral data on excitation and emission bands. This material is available free of charge via the Internet at http://pubs.acs.org.

References

(1) Haes, A. J.; Van Duyne, R. P. *Anal. Bioanal. Chem.* **2004**, *379*, 920−930.
(2) Lakowicz, J. R. *Plasmonics* **2006**, *1*, 5−33.
(3) Ebbesen, T. W.; Lezec, H. J.; Ghaemi, H. F.; Thio, T.; Wolff, P. A. *Nature* **1998**, *391*, 667−669.
(4) Hecht, B.; Sick, B.; Wild, U. P.; Deckert, V.; Zenobi, R.; Martin, O. J. F.; Pohl, D. W. *J. Chem. Phys.* **2000**, *112*, 7761−7774.
(5) Neacsu, C. C.; Steudle, G. A.; Raschke, M. B. *Appl. Phys. B: Lasers Opt.* **2005**, *80*, 295−300.
(6) Sánchez, E. J.; Novotny, L.; Xie, X. S. *Phys. Rev. Lett.* **1999**, *82*, 4014−4017.
(7) Nie, S.; Emory, S. R. *Science* **1997**, *275*, 1102−1106.
(8) Michaels, A. M.; Nirmal, M.; Brus, L. E. *J. Am. Chem. Soc.* **1999**, *121*, 9932−9939.
(9) Kneipp, K.; Kneipp, H.; Izkan, I.; Dasari, R. R.; Feld, M. S. *J. Phys.: Condens. Matter* **2002**, *14*, R597−R624.
(10) Haynes, C. L.; Van Duyne, R. P. *J. Phys. Chem. B* **2003**, *107*, 7426−7433.
(11) Vuckovic, J.; Loncar, M.; Scherer, A. *IEEE J. Quantum Electron.* **2000**, *36*, 1131−1144.
(12) Hobson, P. A.; Wedge, S.; Wasey, J. A. E.; Sage, I.; Barnes, W. L. *Adv. Mater.* **2002**, *14*, 1393−1396.
(13) Chance, R. R.; Prock, A.; Silbey, R. J. *Adv. Chem. Phys.* **1978**, *37*, 1−65.
(14) Barnes, W. L. *J. Modern Opt.* **1998**, *45*, 661−699.
(15) Dulkeith, E.; Ringler, M.; Klar, T. A.; Feldmann, J.; Munoz Javier, A.; Parak, W. J. *Nano Lett.* **2005**, *5*, 585−589.
(16) Dulkeith, E.; Morteani, A. C.; Niedereichholz, T.; Klar, T. A.; Feldmann, J.; Levi, S. A.; van Veggel, F. C. J. M.; Reinhoudt, D. N.; Moller, M.; Gittins, D. I. *Phys. Rev. Lett.* **2002**, *89*, 203002.
(17) Cannone, F.; Chirico, G.; Bizzarri, A. R.; Cannistraro, S. *J. Phys. Chem. B* **2006**, *110*, 16491−16498.
(18) Pan, S. L.; Wang, Z. J.; Rothberg, L. J. *J. Phys. Chem. B* **2006**, *110*, 17383−17387.
(19) Kulakovich, O.; Strekal, N.; Yaroshevich, A.; Maskevich, S.; Gaponenko, S.; Nabiev, I.; Woggon, U.; Artemyev, M. *Nano Lett.* **2002**, *2*, 1449−1452.
(20) Sokolov, K.; Chumanov, G.; Cotton, T. M. *Anal. Chem.* **1998**, *70*, 3898−3905.
(21) Xie, F.; Baker, M. S.; Goldys, E. M. *J. Phys. Chem. B* **2006**, *110*, 23085−23091.
(22) Shimizu, K. T.; Woo, W. K.; Fisher, B. R.; Eisler, H. J.; Bawendi, M. G. *Phys. Rev. Lett.* **2002**, *89*, 117401.

(23) Kühn, S.; Håkanson, U.; Rogobete, L.; Sandoghdar, V. *Phys. Rev. Lett.* **2006**, *97*, 017402.

(24) Anger, P.; Bharadwaj, P.; Novotny, L. *Phys. Rev. Lett.* **2006**, *96*, 113002.

(25) Das, P. C.; Puri, A. *Phys. Rev. B* **2002**, *65*, 155416.

(26) Gersten, J.; Nitzan, A. *J. Chem. Phys.* **1981**, *75*, 1139−1152.

(27) Andreussi, O.; Corni, S.; Mennucci, B.; Tomasi, J. *J. Chem. Phys.* **2004**, *121*, 10190−10202.

(28) Carminati, R.; Greffet, J. J.; Henkel, C.; Vigoureux, J. M. *Opt. Commun.* **2006**, *261*, 368−375.

(29) Thomas, M.; Greffet, J.-J.; Carminati, R.; Arias-Gonzalez, J. R. *Appl. Phys. Lett.* **2004**, *85*, 3863−3865.

(30) Kümmerlen, J.; Leitner, A.; Brunner, H.; Aussenegg, F. R.; Wokaun, A. *Mol. Phys.* **1993**, *80*, 1031−1046.

(31) Ray, K.; Badugu, R.; Lakowicz, J. R. *Langmuir* **2006**, *22*, 8374−8378.

(32) Schneider, G.; Decher, G.; Nerambourg, N.; Praho, R.; Werts, M. H. V.; Blanchard-Desce, M. *Nano Lett.* **2006**, *6*, 530−536.

(33) Zhang, J.; Gryczynski, I.; Gryczynski, Z.; Lakowicz, J. R. *J. Phys. Chem. B* **2006**, *110*, 8986−8991.

(34) Hao, E.; Schatz, G. C. *J. Chem. Phys.* **2004**, *120*, 357−366.

(35) Tam, F.; Goodrich, G. P.; Johnson, B. R.; Halas, N. J. *Nano Lett.* **2007**, http://dx.doi.org/10.1021/nl062901x.

(36) Corrigan, T. D.; Guo, S.; Phaneuf, R. J.; Szmacinski, H. *J. Fluoresc.* **2005**, *15*, 777−784.

(37) Brolo, A. G.; Kwok, S. C.; Moffitt, M. G.; Gordon, R.; Riordon, J.; Kavanagh, K. L. *J. Am. Chem. Soc.* **2005**, *127*, 14936−14941.

(38) Pompa, P. P.; Martiradonna, L.; Della Torre, A.; Della Sala, F.; Manna, L.; De Vittorio, M.; Calabi, F.; Cingolani, R.; Rinaldi, R. *Nat. Nanotechnol.* **2006**, *1*, 126−130.

(39) Song, J.-H.; Atay, T.; Shi, S.; Urabe, H.; Nurmikko, A. V. *Nano Lett.* **2005**, *5*, 1557−1561.

(40) Demers, L. M.; Ginger, D. S.; Park, S.-J.; Li, Z.; Chung, S.-W.; Mirkin, C. A. *Science* **2002**, *296*, 1836−1838.

(41) Mirkin, C. A. *Inorg. Chem.* **2000**, *39*, 2258−2272.

(42) Mock, J. J.; Barbic, M.; Smith, D. R.; Schultz, D. A.; Schultz, S. *J. Chem. Phys.* **2002**, *116*, 6755−6759.

(43) Sherry, L. J.; Jin, R. C.; Mirkin, C. A.; Schatz, G. C.; Van Duyne, R. P. *Nano Lett.* **2006**, *6*, 2060−2065.

(44) Bonacina, L.; Callegari, A.; Bonati, C.; van Mourik, F.; Chergui, M. *Nano Lett.* **2006**, *6*, 7−10.

(45) Jin, R. C.; Cao, Y. W.; Mirkin, C. A.; Kelly, K. L.; Schatz, G. C.; Zheng, J. G. *Science* **2001**, *294*, 1901−1903.

(46) Mirkin, C. A. *MRS Bull.* **2000**, *25*, 43−54.

(47) Herne, T. M.; Tarlov, M. J. *J. Am. Chem. Soc.* **1997**, *119*, 8916−8920.

(48) Mock, J. J.; Smith, D. R.; Schultz, S. *Nano Lett.* **2003**, *3*, 485−491.

(49) Zhou, D. J.; Sinniah, K.; Abell, C.; Rayment, T. *Langmuir* **2002**, *18*, 8278−8281.

(50) Weber, W. H.; Eagen, C. F. *Opt. Lett.* **1979**, *4*, 236−238.

(51) McFarland, A. D.; Young, M. A.; Dieringer, J. A.; Van Duyne, R. P. *J. Phys. Chem. B* **2005**, *109*, 11279−11285.